3) Lan's method. Lan[4] derived the following expression

$$I^{(2)}(x_i)=\frac{\pi}{N}\sum_{k=1}^{N}\frac{1-\xi_k}{x_i-\xi_k}f_k$$

$$\xi_k=-\cos\frac{(2k-1)}{2N}\pi,\qquad x_i=-\cos\frac{i\pi}{N}$$

$$k=1,2,\ldots N,\qquad\qquad i=1,2,\ldots N\tag{15}$$

Lan used the trapezoidal rule for trigonometric variables in place of interpolation functions, as well as Chebychev's polynomial of the first kind. Note that Eq. (15) leads to a scheme different from that in Eqs. (4) and (8) for the layout of loading and upwash points.

Integral $I^{(3)}(x)$

$I^{(3)}(x)$ containing the logarithmic kernel is described by Fromme and Golberg[5] as a pressure mode scheme. But we want it in doublet-lattice scheme. Use of Eq. (10) and the formula

$$\ell n\,|\cos\theta-\cos\varphi|=-2\sum_{n=1}^{\infty}\frac{1}{n}\cos n\theta\cos n\varphi-\ell n2\quad\text{for }\theta\neq\varphi\tag{16}$$

yields

$$I^{(3)}(x)=\sum_{n=0}^{\infty}F_n(\theta)\int_0^{\pi}f(\varphi)\cos n\varphi\,\mathrm{d}\varphi\tag{17}$$

where

$$\begin{aligned}-F_n(\theta)&=\ell n2+\cos\theta, && n=0\\ &=\ell n2+2\cos\theta+\tfrac{1}{2}\cos2\theta, && n=1\\ &=\frac{\cos(n-1)\theta}{n-1}+\frac{2}{n}\cos n\theta+\frac{\cos(n+1)\theta}{n+1}, && n\geq2\end{aligned}\tag{18}$$

Substitution of Eq. (9) into the integral in Eq. (17) gives

$$\int_0^{\pi}f(\varphi)\cos n\varphi\,\mathrm{d}\varphi=\frac{2\pi}{2N+1}\sum_{j=1}^{N}f(\varphi_j)\times\left[\cos n\varphi_j+(-1)^{N+j+n}\sin\frac{\varphi_j}{2}\right]\tag{19}$$

Thus we have

$$I^{(3)}(x)=\sum_{j=1}^{N}A_j^{(3)}(x)f(\xi_j)\quad\text{for }x\neq\xi_j\tag{20a}$$

where

$$A_j^{(3)}(x)=\frac{2\pi}{2N+1}\sum_{n=0}^{N}\left[\cos n\varphi_j+(-1)^{N+j+n}\sin\frac{\varphi_j}{2}\right]F_n(\theta)\tag{20b}$$

In our work on calculations of subsonic nonsteady airfoil loading with the doublet-lattice scheme, the quadrature of Eqs. (20) with $x=x_p$ drastically improves the convergence of solutions. Truncation of the n summation by N is seen to be quite satisfactory in several applications.[6]

References

[1]Hsu, P. T., "Some Recent Developments in the Flutter Analysis of Low-Aspect-Ratio Wings," Paper presented at Institute of the Aeronautical Sciences, National Specialists Meeting, 1958.

[2]Davies, D. E., "Calculation of Unsteady Generalized Air Forces on a Thin Wing Oscillating Harmonically in Subsonic Flow," British Aeronautical Research Council, R&M 3409, 1965.

[3]Stark, V.J.E., "A Generalized Quadrature Formula for Cauchy Integrals," *AIAA Journal*, Vol. 9, Sept. 1971, pp. 1854-1855.

[4]Lan, C. E., "A Quasi-vortex-Lattice Method in Thin Wing Theory," *Journal of Aircraft*, Vol. 11, Sept. 1974, pp. 518-527.

[5]Fromme, J. and Golberg, M., "Unsteady Two-Dimensional Airloads Acting on Oscillating Thin Airfoils in Subsonic Ventilated Wind Tunnels," NASA CR 2967, 1978.

[6]Ando, S. and Ichikawa, A., "The Use of an Error Index to Improve Numerical Solutions for Unsteady Lifting Airfoils," *AIAA Journal*, Vol. 21, Jan. 1983, pp. 47-54.

Freestream Turbulence and Transonic Flow over a "Bump" Model

S. Raghunathan* and R.J.W. McAdam†
The Queen's University of Belfast, Northern Ireland

Nomenclature

C_p = nondimensional pressure coefficient
ℓ_s = separated flow length
M_{pk} = peak Mach number on the model
M_∞ = freestream Mach number measured two chords upstream of model leading edge
R_θ = Reynolds number based on θ
R_δ = Reynolds number based on δ
Tu_∞ = freestream turbulence intensity 6 mm upstream of the shock location, $\tilde{u}/U_\infty$
X = distance measured from leading edge of the model
X_s = shock position measured from the leading edge of the model
X_{s0} = shock position at zero turbulence intensity
$\tilde{u}$ = root mean square velocity fluctuation
U_∞ = freestream velocity 6 mm upstream of the shock location
δ = boundary-layer thickness 6 mm upstream of the shock location
δ^* = boundary-layer displacement thickness 6 mm upstream of the shock location
θ = boundary-layer momentum thickness 6 mm upstream of the shock location

Introduction

IN transonic flow, predictions of free-flight conditions from wind tunnel tests need a close simulation of Reynolds number. However, Reynolds number simulation is not adequate, since results from wind tunnel tests are influenced by effects of tunnel environment, such as noise and turbulence levels.[1] A recent paper by the authors[2] showed a strong influence of turbulence on attached turbulent boundary layers at zero pressure gradient in the Mach number range of 0-0.8 and boundary-layer momentum thickness Reynolds number range of 3000-10^4. This Note presents the general characteristics of transonic flow over a "bump" model at various freestream turbulence levels.

Received Nov. 19, 1981; revision received June 22, 1982.

*Lecturer, Department of Aeronautical Engineering. Member AIAA.
†Research Student, Department of Aeronautical Engineering.

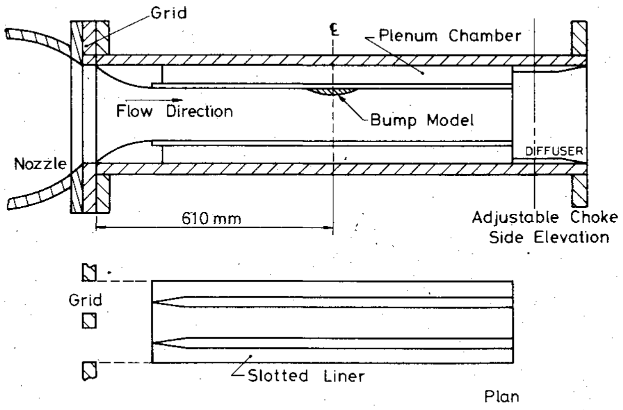

Fig. 1 Schematic diagram of the test setup.

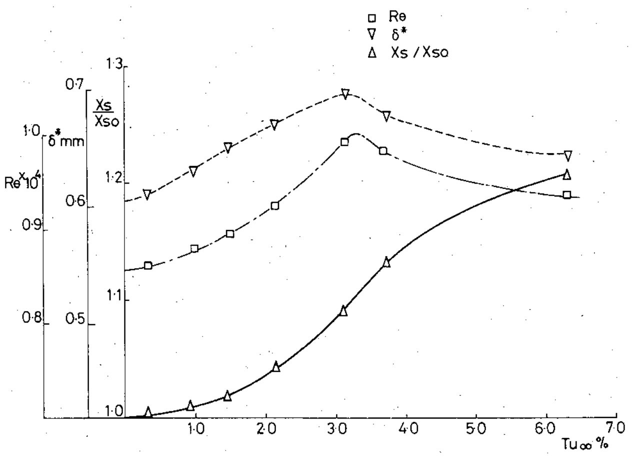

Fig. 2 Variation of shock position, boundary-layer displacement thickness and momentum thickness Reynolds number with turbulence.

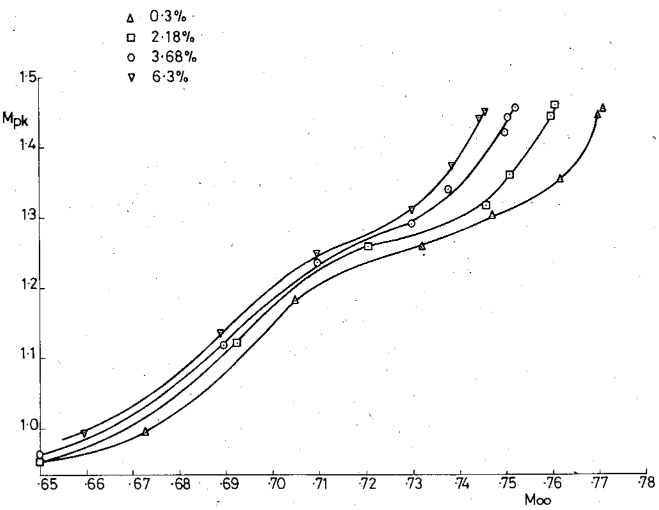

Fig. 3 Influence of turbulence on peak Mach number.

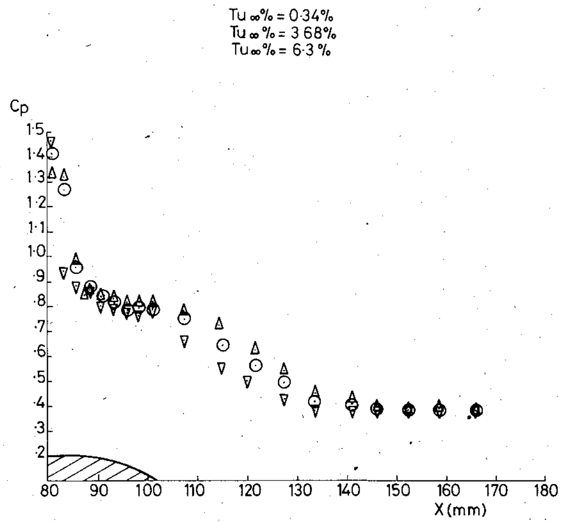

Fig. 4 Pressure distribution in the shock-induced separation.

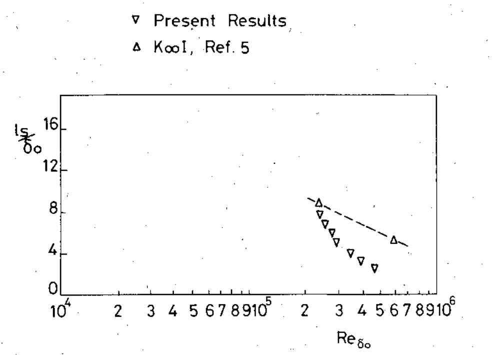

Fig. 5 Variation of separation length with Reynolds number.

Tests

The tests were performed in a 10 cm² transonic suck-down tunnel with a slotted floor test section. The slots were covered with screens giving overall porosity of 2.4% based on all four walls of the test section. The bump model was a half circular arc airfoil 9% thick and 10 cm chord length mounted on the test section roof as shown in Fig. 1. The model had pressure orifices on the centerline located at 5 and 2.5 mm intervals over the front and the rear half, respectively. Pressure orifices also were located on the tunnel side wall upstream and downstream of the model and on the tunnel roof downstream of the model. The freestream turbulence was varied by monoplane grids placed well upstream of the model location. Earlier pitot and hot-wire measurements have shown that the boundary layer on the roof surface was fully turbulent from the position where the monoplane grids were placed and the freestream turbulence at the model location was free from the vortex shedding due to the grids. The scale of freestream turbulence L_ϵ was of the same order as the boundary-layer thickness δ. The details of the turbulence measurements including spectra are given in Ref. 2. Measurements were made of the pressure distribution over the model in the Mach number range of 0.65-0.78 and in the freestream turbulence level range of 0.3-6%. For a constant shock Mach number of 1.44 and for various turbulence levels, measurements were also made at the velocity profiles upstream of the shock. The china clay flow visualization technique was used to measure the separation length.

Results and Discussions

The influence of freestream turbulence Tu_∞ on the shock position over the model for a constant freestream Mach number of $M_\infty = 0.745$ is shown in Fig. 2. The shock positions X_s are normalized with respect to the extrapolated value of the position of shock X_{s0} at zero turbulence level. The boundary-layer momentum thickness Reynolds number R_θ and boundary-layer displacement thickness δ^* measured just before the shock are also shown in the figure. It is observed that an increase in Tu from 0.3 to 6% produces a shift in the shock position of 20%. Such a large change in the shock position cannot be explained solely in terms of the thickening of the boundary layer associated with the increase in freestream turbulence. First, the initial increase in δ^* followed by a decrease is not likely to produce such a large shift in the shock position in one direction. This is shown by the experiments performed by Delery[3] on a similar model and at a constant freestream turbulence level. Second, R_θ does not increase continuously with the increase in Tu_∞, whereas the shock position shifts in only one direction with the increase in Tu_∞. Typically, Tu_∞ levels of 2.5 and 5.1% produce the same value of R_θ, whereas the shock positions for these two values of R_θ are not the same. It appears that the freestream turbulence has a direct effect on the shock interactions and, therefore, the shock position.

Figure 3 shows the influence of Tu on the peak Mach number on the model M_{pk}. The influence of Tu_∞ on M_{pk} is larger at $M_{pk} \gtrsim 1.3$, a condition corresponding to significant shock-induced separation. This suggests that the freestream turbulence plays an important part in strong adverse pressure gradients where large regions of separation are present.

The pressure distributions in the region of shock-induced separation for a constant value of $M_{pk} = 1.44$ and for various freestream turbulence levels Tu are shown in Fig. 4. The differences in C_p levels at the shock position are due to the differences in the freestream Mach numbers needed to achieve a constant value of M_{pk}. The shock position at this value of M_{pk} is typically 80% chord. Increase in Tu_∞ is shown to produce an increase in pressure recovery at the trailing edge of the model. Similar trends in C_p have been observed with the introduction of vortex generators.[4] The increase in pressure recovery is due to the increase in momentum transport from the freestream into the separated region produced by the turbulence.

China clay flow visualization showed a two-dimensional separation over 90% of the model span. Figure 5 shows the variation of separation length, nondimensionalized with respect to the boundary-layer thickness measured upstream of the shock, with the Reynolds number based on the boundary-layer thickness. When compared with the results of Kooi[5] it is seen that for given boundary-layer conditions upstream of the shock wave, the separation length is influenced by the freestream turbulence.

Thus it can be concluded that the freestream turbulence plays an important part in transonic flow with shock interactions. Detailed measurements of flowfield at various levels of the freestream turbulence are in progress.

References

[1] Green, J.E., "On the Influence of Free Stream Turbulence on a Turbulent Boundary Layer as it Relates to Wind Tunnel Testing at Subsonic Speeds," AGARD Report 602, 1973 and RAE TR 72201, 1972.

[2] Raghunathan, S. and McAdam, R.J.W., "Free Stream Turbulence and Attached Subsonic Turbulent Boundary Layer," AIAA Paper 82-0029, Jan. 1982.

[3] Delery, J., "Some Features of Transonic Shock Wave Turbulent Boundary Layer Interaction," *Shock Boundary Layer Interactions in Turbomachines,* Von Kármán Institute Lecture Series, Brussels, No. 8, 1980, pp. 1-17.

[4] Green, J.E., "Interactions between Shock Waves and Turbulent Boundary Layers," RAE TR 69098, May 1969.

[5] Kooi, J.W., "Influence of Free Stream Mach Number on Transonic Shock Wave Boundary Layer Interaction," NLR MP 78013u, 1978.

Dynamic Stability Boundaries for a Sinusoidal Shallow Arch under Pulse Loads

Michael T. Donaldson* and Raymond H. Plaut†
Virginia Polytechnic Institute and State University, Blacksburg, Virginia

Introduction

THE dynamic snap-through of a shallow elastic arch subjected to triangular pulse loads is investigated. Concentrated loads with independent magnitudes are applied at the quarter points of the arch as a means of assessing the effects of load asymmetry. Critical load combinations are determined and the effects of the pulse duration and external damping on the interaction curves are examined. The behavior is similar to that of some shallow shells under blast loads and demonstrates that asymmetric loading may have much lower critical values than symmetric loading.

Humphreys[1] and Fulton and Barton[2] investigated the instability of arches subjected to rectangular pulse loads. External damping was considered by Lock[3] and Hegemier and Tzung,[4] whereas Huang and Nachbar[5] and Johnson[6] treated material damping with a Kelvin-Voigt model. Step loads were applied in Refs. 3-5 and impulse loads in Ref. 6. Interaction curves for multiple step loads were presented by Gregory and Plaut.[7]

Analysis

The ends of the arch are simply supported, the unloaded configuration is

$$Y_0(X) = \Lambda \sin(\pi X/L) \qquad 0 \leq X \leq L \tag{1}$$

and the shape at time T is $Y(X,T)$. The arch has mass μ per unit length, Young's modulus E, cross-sectional area A, moment of inertia I, and radius of gyration $r = \sqrt{I/A}$. Concentrated downward loads $P_1(T)$, $P_2(T)$, and $P_3(T)$ are applied at $X = L/4$, $L/2$, and $3L/4$, respectively. The coefficient of external damping is denoted C.

Consider the nondimensional quantities

$$x = X/L \qquad y = Y/(2r) \qquad y_0 = Y_0/(2r)$$
$$\lambda = \Lambda/(2r) \qquad t = T\sqrt{EI/(\mu L^4)} \qquad c = CL^2/\sqrt{EI\mu}$$
$$p_k = P_k L^3/(2\pi^4 EIr) \qquad k = 1,2,3 \tag{2}$$

and let the downward deflection be denoted by w, i.e.,

$$w(x,t) = y_0(x) - y(x,t) \tag{3}$$

The equation of motion under the standard shallow-arch assumptions is[1]

$$\frac{\partial^2 w}{\partial t^2} + c\frac{\partial w}{\partial t} + \frac{\partial^4 w}{\partial x^4} + m\frac{\partial^2 (w - y_0)}{\partial x^2} = \pi^4 \sum_{k=1}^{3} p_k \delta[x - (k/4)] \tag{4}$$

Received Oct. 9, 1981; revision received Feb. 17, 1982.

*Graduate Student, Department of Civil Engineering, presently with Exxon Research and Engineering Co., Florham Park, N.J.
†Professor, Department of Civil Engineering.